# Nonadiabatic ab Initio Dynamics of Two Models of Schiff Base Retinal†

**Toshimasa Ishida***

*Fukui Institute for Fundamental Chemistry, Kyoto University, 34-4, Takano-nishihirakicho, Kyoto 606-8103, Japan*

**Shinkoh Nanbu**

*Research Institute for Information Technology, Kyushu University, Hakozaki 6-10-1, Higashi-ku, Fukuoka, 812-8581, Japan*

**Hiroki Nakamura**

*Institute for Molecular Science, National Institutes of Natural Sciences, Myodaiji, Okazaki, 444-8585, Japan*

*Received: December 14, 2008; Revised Manuscript Received: February 1, 2009*

On-the-fly classical dynamics calculations combined with ab initio quantum chemical computations are carried out for two models of protonated Schiff base retinal in vacuo. The models are the 6$\pi$ system of 2-*cis*-penta-2,4-dieneimminium cation and the 12$\pi$ system in which two methyl groups are removed from the Schiff base of retinal. The CASSCF(6,6) level with the 6-31G basis set was employed for the quantum chemical part and the velocity Verlet algorism is utilized for time evolution of trajectories. The probabilities of nonadiabatic transition between the excited and ground state are estimated by the Zhu−Nakamura formulas. The 9-cis form product in addition to the all-trans one is generated in the present gas phase calculation for the 12$\pi$ model, despite the 9-cis generation being suppressed in protein. We have found that energy relaxation on the ground state occurs in two steps in the 12$\pi$ model. In the first step a metastable intermediate state is formed at ∼100 fs after photoexcitation at the energy around 20−40 kcal/mol down from the excited potential energy surface, then it further relaxes to the energy around 60−80 kcal/mol from the excited surface, leading to the final state (second step). This relaxation pattern can be seen in all the three pathways to the all-trans, 9-cis, and (reverted) 11-cis form. Fourier transformation analysis reveals that the effective vibrational frequencies of the intermediate state are 1600−2000 $cm^{-1}$, which can be attributed to the conjugate CC bond frequencies in the electronic ground state. The two-step relaxation may be due to dynamical barriers. The two-step relaxation is not revealed in the smaller 6$\pi$ model. The crank-shaft motion of the C11═C12 and C9═C10 bonds is found in the isomerization, which indicates the motion is intrinsic in retinal, not due to the surrounding protein. The branching ratio is about 1:1:2 for the all-trans, 9-cis, and 11-cis form generation. The ratio is different from earlier works where Tully's fewest switching scheme was employed. The bond length and the dihedral angle at the transitions are also analyzed to investigate the transition mechanism.

## Introduction

Retinal is embedded in rhodopsin protein, which is responsible for the vision of vertebrate animals including humans. When the retinal is exposed to light, the 11-cis form is excited and isomerized to the all-trans form. This process has been investigated experimentally as well as theoretically.[1−5] Vreven and Morokuma applied the ONIOM methods to obtain the $S_1$ energy profile.[6] Frutos et al. calculated a QM/MM trajectory in rhodopsin protein and found that a complex change of the retinal backbone initiates "asynchronous bicycle-pedal or crankshaft" motion.[7] They analyzed only one trajectory, which is definitely not good enough to investigate the mechanism. Weingart et al. carried out ab initio molecular dynamics in vacuo using five double-bond models and also found the crankshaft motion.[8,9]

In this article, we investigate nonadiabatic classical dynamics of retinal in vacuo, mainly the energy relaxation after the transition to the ground state. We employ two model systems of 6$\pi$ and 12$\pi$ to investigate the isomerization to examine how the model size affects the energy relaxation mechanism. Tens to one hundred trajectories are calculated.

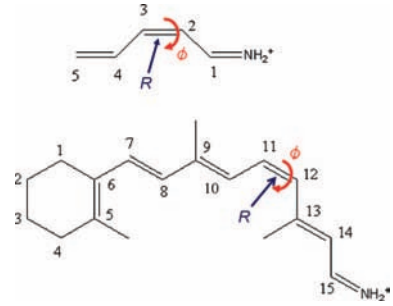


**Figure 1.** The molecular structures of two models considered: the 6$\pi$ system of 2-*cis*-penta-2,4-dieneimminium cation ($CH_2$═CH−CH═CH−CH═$NH_2^+$) and the 12$\pi$ system in which two methyl groups are removed from position 1 of the Schiff base of retinal. The numbers attached to the structures show the positions of carbons.

The two systems considered are shown in Figure 1. The 6$\pi$ model system is the 2-*cis*-penta-2,4-dieneimminium cation ($CH_2$═CH−CH═CH−CH═$NH_2^+$) or protonated Schiff base 3

† Part of the "George C. Schatz Festschrift".

* Corresponding author. E-mail: ishida@fukui.kyoto-u.ac.jp.

10.1021/jp8110315 CCC: $40.75 
Published on Web 03/19/2009

(PSB3) and the 12$\pi$ system is the PSB of retinal, in which two methyl groups are removed from position 1 of the base for computational affordability. The 6$\pi$ and 12$\pi$ models consist of 12 and 45 atoms and the number of degrees of freedom in the two models is 30 and 129.

By comparing the difference between the simple model and the realistic one, we have found that a two-step relaxation occurs in the ground state only in the case of the larger 12$\pi$ model, whereas the smaller 6$\pi$ system shows no significant two-step relaxation.

The nonadiabatic transitions are treated by the Zhu−Nakamura formulas.[10−13] The Landau−Zener−Stückelberg formula[14] has been used widely to treat nonadiabatic transitions, but the Zhu−Nakamura formulas are far more versatile and accurate, being applicable at any energy, and are yet very simple.

There are several models to describe motion of retinal backbone for cis−trans isomerization of retinal. Kakitani et al. proposed the one-bond rotation model and interpreted absorption and circular dichroism spectra.[15] Warshel proposed the bicycle pedal model in which cis−trans isomerization occurs one after another and the cis-position moves to the tail to give the all-trans form.[16] The Hula-twist model is proposed by several research groups in which the single bond next to the relevant double bond rotates together.[17−19] Yamada et al. proposed the twist sharing model, a sophistication of the one-bond model, in which single and double bonds near the relevant double bond rotate a little bit to the direction opposite to the relevant bond.[20] Frutos et al. proposed the "asynchronous bicycle-pedal or crankshaft" model[7] and, Weingart et al. found the crankshaft motion in the five-double-bond model in vacuo without the $\beta$-ionone ring.[8] The present result in vacuo supports the idea of the crankshaft motion of these two reports, in which the −C9═C10− bond rotates in the direction opposite to the −C11═C12− bond. Thus, the −C9═C10− twist is not due to a steric constraint imposed by the protein environment, but is intrinsic in retinal itself, as Weingart pointed out.

It is found that the 9-cis form product in addition to the all-trans one is generated in the present gas phase calculation for the 12$\pi$ model, despite the 9-cis generation being suppressed in the rhodopsin protein. The 9-cis form is the chromophore of isorhodopsin. Strambi et al. calculated the relaxation path of isorhodopsin and discuss the relationship with the path of rhodopsin.[21] The pathway of the 11-cis to 9-cis form in vacuo found here would also shed light on the relationship.

## Calculations

On-the-fly classical dynamics calculations combined with ab initio quantum chemical computations were carried out in which nonadiabatic transitions are taken into account. The state-averaged 6 electron 6 orbital complete active space self-consistent field (CAS(6,6) SCF) scheme with the 6-31G basis set are employed for the electronic part of the calculations for both systems. In general, the larger the active space employed the better the results. We had to compromise at a certain level, however, since the CPU time becomes unrealistically large. Typically, one trajectory in the 12$\pi$ system takes about two months with the AMD Opteron 2.2 GHz CPU employed. We carried out CAS(12,12) calculation for comparison at the initial geometry. The $S_0-S_1$ transition dipole moments are 11.3 and 14.4 debye for the CAS(6,6) and CAS(12,12) wave functions. The dipole moments of $S_1$ are 33.3 and 36.9 debye. The excitation energies are 81.0 and 52.1 kcal/mol. The smaller excitation energy in CAS(12,12) would be due to the better description of electron correlation. The overestimation of the energy is taken into account when the lifetime is deduced later. In the CAS(12,12) wave function, analysis of configuration state functions (CSF) of CAS(12,12) revealed that all the CSFs with coefficients larger than 0.06 are included in the CAS(6,6) CSF. Thus, the description by the CAS(6,6) wave function would be semiquantitatively correct in comparison with the case of CAS(12,12).

The lowest three states were used for the CAS averaging for the 6$\pi$ system, and we found that the transitions essentially occur between the two lower states. Thus, in order to reduce the computational cost we employed the two lowest states in the 12$\pi$ systems for the CAS averaging. We have confirmed that we are working on the correct excited state as follows. The relevant $S_1$ state is described essentially by the HOMO−LUMO excitation and bright, because the $S_0-S_1$ transition dipole moment is as large as 11.3 debye. The HOMO and LUMO are $\pi$-orbitals which have polarized distributions to the $\beta$-ionene ring and to the Schiff base, respectively. The $S_1$ state, therefore, has a charge transfer character, and its dipole moment is 33.3 debye.

The program suites Molpro 2006.1 and 2002.6 were used for electronic structure calculations.[22,23] Gaussian 03 was also used for optimization of several important geometries, including conical intersections.[24] For the 6$\pi$ system, molecular orbitals were reordered so that all six $\pi$ orbitals were included in the CAS active space at the initial geometry, which assured that the three vacant $\pi$ orbitals were in the active space during the time evolution of trajectories. In the case of 12$\pi$ system, the six orbitals located from HOMO-2 to LUMO+2 were chosen as the active space and we confirmed that all six orbitals have $\pi$-character.

The velocity Verlet algorithm was used to run trajectories of nuclear motion.[25] The initial geometry of the ground state is the one optimized by the B3LYP method. The DFT-based structure still has the correct bond alternation and is believed to be qualitatively correct, although it may underestimate the alternation. We represent the coordinate distribution by a single optimized geometry for coordinates. This comes from the fact that the maximum value of the distribution is located very close to the optimized geometry. The initial velocity was given randomly according to the Boltzmann distribution at $T = 300$ K and the molecule was excited onto the first excited state. One may want to choose the Wigner distribution, but the Wigner distribution with 0 K would not necessarily be the best one. Thus, we chose the Boltzmann distribution with a finite temperature for velocity distribution. The time step used is 0.5 fs. This might be somewhat large, but it is a compromise between accuracy and reasonable execution time. Forty-one and ninety-eight trajectories were calculated for the 6$\pi$ and 12$\pi$ systems, respectively.

The surface hopping procedure is based on the Zhu−Nakamura theory, which provides a complete set of solutions for the curve-crossing problem, covering the whole energy range. The multidimensional surface hopping scheme using the Zhu−Nakamura formulas has been applied to several systems successfully and reproduced quantum mechanical results for cumulative reaction probabilities for $H_2 + H^+$,[26,27] $H_2 + D^+$,[27−29] and $C + H_2$[30] except for oscillatory resonance structures. In addition, Li et al. calculated the cross sections for $H_2 + H^+$ and $H_2 + D^+$ which are in agreement with the experiments.[27] Feng et al. employed the Zhu−Nakamura theory to investigate selectivity of bond fissions of photodissociation of bromoacetyl chloride with combined nonadiabatic Rice−Ramsperger−

Kassel−Marcus theory and ab initio molecular dynamics calculations.[31] They found that nonadiabatic transitions play important roles in determining selective dissociations of the C−Cl and C−Br bonds. The present implementation is based on the generalized trajectory surface hopping method of ref 30. The information needed is adiabatic potential energies and forces at each time step. The nonadiabatic coupling vectors are evaluated to determine the transition direction only when the probability would be significant, i.e., when the adiabatic energy difference between the two adjacent surfaces becomes minimum.

The procedure is summarized as follows. When the energy difference between the two adjacent adiabatic potential energy surfaces is a local minimum, the nonadiabatic coupling vector is calculated. The one-dimensional adiabatic potential curves are calculated in the direction of the coupling vector and the type of crossing is identified: nonadiabatic tunneling type or Landau−Zener type. In the former, the signs of the potential slopes are different, while in the latter, the two potential curves cross with the same sign of slope. The transition probability is estimated by using the Zhu−Nakamura formulas from the adiabatic potentials. The transition probability calculated is compared to a uniform random number generated and the decision is made whether the transition to the adjoining surface occurs or the trajectory stays on the same surface. A nonvertical hop, which corresponds to a classically forbidden transition, is taken into account when the kinetic energy is not enough for the vertical hop, which corresponds to classically allowed transition. Thus, classically forbidden transitions can also be properly taken into account, although such transitions are found not to be encountered very much in the present systems. The classically allowed transitions at the energies near the crossing point occur rather frequently and can be accurately treated in the present scheme.

Trajectories were evolved 50 more steps after the absolute value of the dihedral angle for the original cis-position reaches 0° or 180° on the ground state. These trajectories are identified as those returned to the cis form (in the case 0°) or those leading to the trans form (180°). For the 12$\pi$ system, the 9-cis (11-trans) form is also generated in addition to the 11-cis and all-trans forms. All the trajectories considered were identified to one of the products on the ground state within 450 fs after the photoexcitation for both 6$\pi$ and 12$\pi$ systems.

## Results and Discussion

**A. Time Evolution of Energy Difference and of Length and Angle of the Twisting Bond.** The energy diagram relevant for the present system is shown in Figure 2. In the 12$\pi$ system of Figure 2a, the 11-cis form is slightly (0.5 kcal/mol) higher than the most stable all-trans form. The 9-cis form is 5.9 kcal/mol higher than the all-trans form. The $S_1$ state is located 82.3, 88.2, and 83.7 kcal/mol above the all-trans equilibrium geometry for the all-trans, 11-cis, and 9-cis forms, respectively. The conical intersection (CI) between the all-trans and 11-cis forms corresponding to the rotation in the rhodopsin protein is located at 68.1 kcal/mol above. The CI between the 11-cis and 9-cis forms is located at 52.6 kcal/mol. Thus, the 9-cis form in addition to the all-trans form is accessible from the 11-cis form after photoexcitation. In the 6$\pi$ system of Figure 2b, the excitation energies are higher than those in the 12$\pi$ system. The geometries at CI are shown in Figure 3. In all the geometries, the relevant bond are twisted about 90°. The bond lengths and dihedral angles for backbone CC and CN bonds for the minima and CI structures are listed in Tables 1 and 2 for the 12$\pi$ and 6$\pi$ systems.

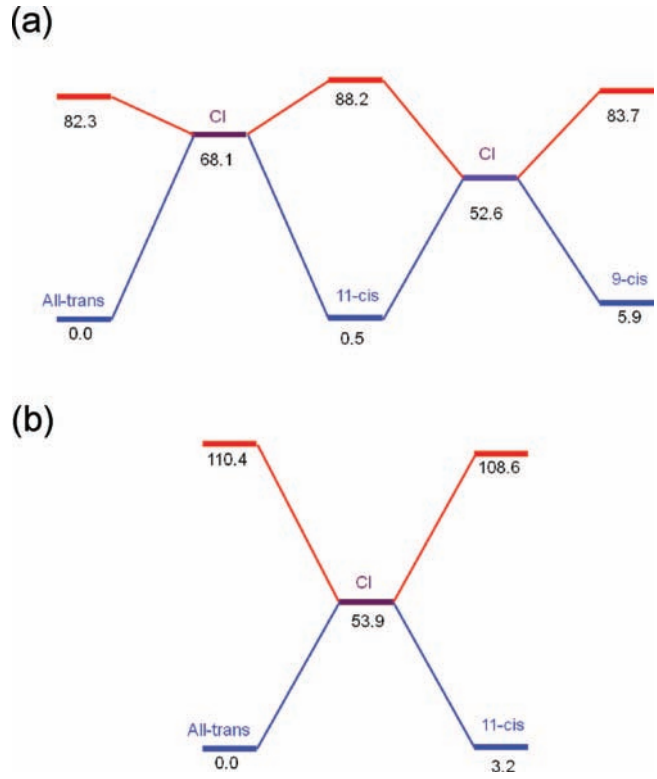


**Figure 2.** Enegy diagram for cis−trans isomerization of retina for the (a) 12$\pi$ and (b) 6$\pi$ system. Energy is in kcal/mol. The blue and red lines indicate the ground and excited states. CI stands for conical intersection.

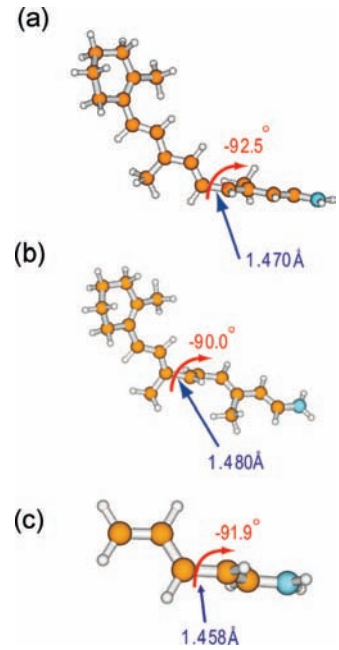


**Figure 3.** Geometries of conical intersections (a, b) between the ground and first excited state [(a) between 11-cis and all-trans forms for the 12$\pi$ system, (b) between 11-cis and 9-cis forms for the 12$\pi$ system] and (c) for the 6$\pi$ system.

Figure 4 shows the time evolution of potential energy difference between the ground and excited states along each trajectory. Note that when the relevant trajectory is on the excited state, the energy is taken to be positive while the value is taken to be negative when the trajectory runs on the ground state. It is revealed that the energy relaxation on the ground state occurs in two steps in the case of the 12$\pi$ model, as is

**TABLE 1: Bond Lengths and Dihedral Angles of Backbone CC and CN Bonds for Minimum Structures in the Ground State and Conical Intersections (CI) in the Excited State for the 12$\pi$ System**

| | all-trans | 11-cis | 9-cis | CI (11c-t)[a] | CI (9c−11c)[b] |
|---|---|---|---|---|---|
| | | | bond lengths[c] | | |
| C5=C6 | 1.355 | 1.355 | 1.355 | 1.334 | 1.344 |
| C6−C7 | 1.483 | 1.483 | 1.484 | 1.492 | 1.464 |
| C7=C8 | 1.334 | 1.334 | 1.333 | 1.409 | 1.394 |
| C8−C9 | 1.458 | 1.459 | 1.460 | 1.393 | 1.398 |
| C9=C10 | 1.382 | 1.386 | 1.382 | 1.481 | 1.480 |
| C10−C11 | 1.412 | 1.413 | 1.412 | 1.327 | 1.370 |
| C11=C12 | 1.389 | 1.396 | 1.389 | 1.470 | 1.428 |
| C12−C13 | 1.409 | 1.412 | 1.409 | 1.490 | 1.393 |
| C13=C14 | 1.396 | 1.398 | 1.396 | 1.350 | 1.414 |
| C14−C15 | 1.381 | 1.382 | 1.381 | 1.431 | 1.373 |
| C15=N16 | 1.320 | 1.319 | 1.320 | 1.285 | 1.331 |
| dihedral angle[d] | | | | | |
| C4−C5=C6−C7 | 179.0 | 178.9 | 178.6 | 178.6 | −179.9 |
| C5=C6−C7=C8 | 58.3 | 58.7 | 60.8 | 75.3 | 43.1 |
| C6−C7=C8−C9 | 177.4 | 177.3 | 177.4 | 176.8 | 178.9 |
| C7=C8−C9−C10 | −179.4 | −179.1 | −179.2 | 179.9 | −176.9 |
| C8−C9=C10−C11 | 179.9 | 180.0 | 0.1 | −179.7 | −90.0 |
| C9=C10−C11=C12 | −179.9 | −179.7 | 179.9 | −177.8 | 179.6 |
| C10−C11=C12−C13 | −180.0 | 0.5 | −179.9 | −92.5 | 12.6 |
| C11=C12−C13=C14 | −180.0 | −179.9 | 180.0 | 169.2 | −177.7 |
| C12−C13=C14−C15 | 180.0 | −180.0 | −180.0 | −179.2 | 178.8 |
| C13=C14−C15=N16 | −180.0 | −179.9 | 180.0 | 179.0 | −179.1 |

[a] The $S_1-S_0$ conical intersection between the all-trans and 11-cis forms. [b] The $S_1-S_0$ conical intersection between the 9-cis and 11-cis forms. [c] In angstroms. [d] In degrees.

**TABLE 2: Bond Lengths and Dihedral Angles of Backbone CC and CN Bonds for Minimum Structures in the Ground State and Conical Intersections (CI) for the 6$\pi$ System**

| | trans | cis | CI |
|---|---|---|---|
| | bond length[a] | | |
| C1=C2 | 1.352 | 1.352 | 1.380 |
| C2−C3 | 1.437 | 1.442 | 1.400 |
| C3=C4 | 1.370 | 1.372 | 1.458 |
| C4−C5 | 1.415 | 1.418 | 1.378 |
| C5=N6 | 1.301 | 1.301 | 1.333 |
| dihedral angle[b] | | | |
| C1=C2−C3=C4 | 180.0 | 180.0 | −178.8 |
| C2−C3=C4−C5 | −180.0 | 0.0 | −91.9 |
| C3=C4−C5=N6 | 180.0 | 180.0 | −179.4 |

[a] In angstroms. [b] In degrees.

shown in Figure 4a. In the 12$\pi$ model, all-trans, 9-cis, and 11-cis forms are generated in the present calculation in vacuo, although the 9-cis form is not observed in rhodopsin protein.[32] This suggests that the generation of the 9-cis form is prevented by the protein environment. The first step lasts for about 130 fs from 70 to 200 fs with the energy difference oscillating between −10 and −50 kcal/mol. The second step is much shorter with the energy oscillation between −70 and −100 kcal/mol and leads to the final state. This relaxation pattern can be seen in the all-trans product form as well as in the reverted 11-cis form, although the duration of the first step is shorter in the latter. The two-step relaxation is not revealed in the smaller 6$\pi$ model as seen in Figure 4b.

The average times of transition after photoexcitation in the 12$\pi$ system are 125, 107, and 118 fs for the all-trans, 9-cis, and 11-cis forms and the overall average is 118 fs. The times for the 6$\pi$ system are 105, 116, and 110 for the trans form, cis form, and all the products. Frutos et al. found that the CASSCF/AMBER potential energy profile is much steeper than the CASPT2//CASSCF/AMBER profile in their trajectory calculation in protein rhodopsin and found that a scaling of the CASSCF/AMBER energy profile leads to a good agreement with the CASPT2//CASSCF/AMBER energy and that the transition time after photoexcitation turns out to be ∼110 fs.[7] They argued that the time for CASSCF trajectories should be scaled by $(0.795)^{-1/2}$ to obtain the CASPT2 time. If this were still the case in our calculations, the average time of transitions for the 12$\pi$ system would be 132 fs. Weingart reported an averaged lifetime of 61 fs for his five-double-bond models.[8] The present result is close to the transition time of Frutos et al. and is larger than the value of Weingart and an experimental value of 50 fs, which was estimated by analysis of a quantum yield.[33] The three calculation values are in the order of the model size considered. The transition time for the 12$\pi$ system of 118 fs is larger than that for the 6$\pi$ system of 110 fs in the present study. The system complexity would affect the transition time.

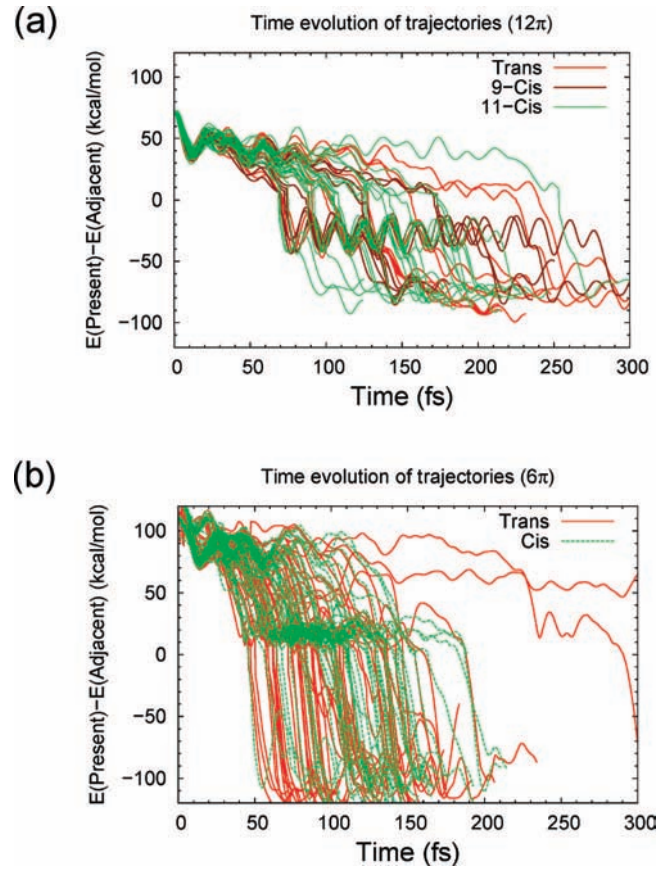


**Figure 4.** Time evolution of energy difference between the ground and first excited state for each trajectory: (a) the 12$\pi$ system and (b) the 6$\pi$ system. Note that when the relevant trajectory is on the excited potential energy surface, the energy difference is taken to be positive, and that when the trajectory is on the ground potential energy surface, the value is taken to be negative. The initial state right after photoexcitation is the cis form.

We also examined time evolution of the twist angle $\phi$ and the length $R$ of the twisting bond. The twisting bond is $C_2-C_3$ for the 6$\pi$ system and $C_{11}-C_{12}$ for the 12$\pi$ system. Figure 5 shows the time evolution of $\phi$. The change of $\phi$ for the 12$\pi$ system is slower than that for the 6$\pi$ system because of the complexity of the 12$\pi$ system. The present "realistic" 12$\pi$ system can still rotate both directions because of the absence of surrounding protein.

Time evolution of the twisting bond $R$ shows that $R$ becomes longer after excitation and shorter after the transition in both systems, reflecting conversion to the single bond by photoex-

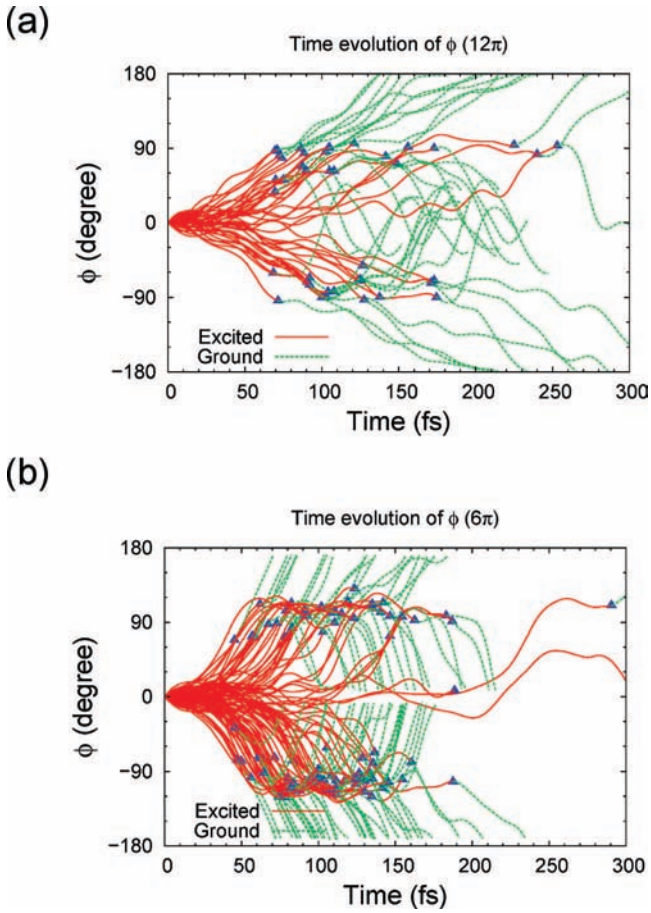


**Figure 5.** Time evolution of the dihedral angle of the twisting bond for (a) the $12\pi$ system and (b) the $6\pi$ system.

citation and returning to the double bond after transition. The bond elongation on the excited state before the relaxation has been reported in the literature for the $6\pi$ system.[34] These results are clearly seen in Figure 6. This figure shows the time evolution of the twisting-bond length $R$ and the signed energy difference for the three trajectories leading to the all-trans and 9-cis form products and going back to the 11-cis form reactant. These three trajectories are typical ones to show two-step relaxation clearly. The signed energy difference is the same as the ordinate axis in Figure 4. It is found in the $12\pi$ system that the length of about 1.45−1.55 Å in the first (intermediate) step is longer than the length of around 1.35−1.45 Å in the second step and is similar to that in the excited state. Since the typical bond lengths of CC single and double bonds are 1.54 and 1.34 Å,[35] the bond in the intermediate step has character close to that of a single bond. Elongation of the twisting bond occurs on the excited surface also. Namely, the twisting double bond becomes single-bond-like before the transition. This two-step change in the excited state is consistent with the two-mode model proposed by González-Luque et al. based on their calculation result for 4-*cis*-$\gamma$-methylnona-2,4,6,8-tetraeniminium cation in vacuo.[36]

The whole process mentioned above from photoexcitation to a stabilized product is summarized in Scheme 1 as follows:

(1) After the photoexcitation, the twisting bond gets longer and becomes like a single bond. (2) The bond twists to the twist angle of around 60−100°. (3) The transition occurs into the ground state. (4) The twisting bond vibrates about 100 fs keeping the single bond character. (5) The energy relaxes further, the twisting bond shrinks to the double bond, and the molecule is finally stabilized in the trans or cis form.

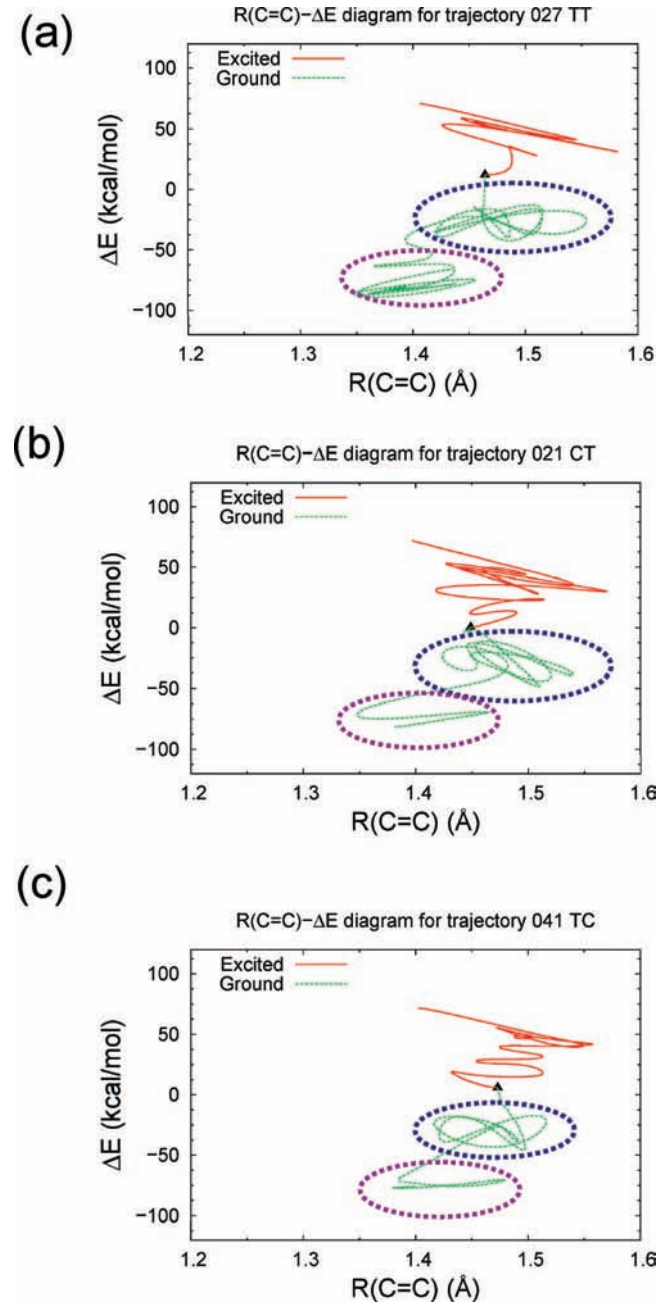


**Figure 6.** Change of the bond length $R$ between $C_{11}$ and $C_{12}$, which is twisted during the cis−trans isomerization, against the energy difference for a typical trajectory producing (a) the all-trans form, (b) the 9-cis form, and (c) the 11-cis form products in the $12\pi$ system. The blue and purple dotted circles indicate the parts of the trajectory which correspond to the intermediate state and the final stabilized state, respectively, although the circles are somewhat arbitrary.

To obtain information on effective vibrational frequencies of the intermediate state, we have carried out a Fourier transformation of trajectories after transition. The time windows used for the Fourier transformation are shifted along trajectories measured from the moment of transition, which is taken to be a time delay of 0. For each time window, the hamming filter function[37]

$$w(n) = 0.54 - 0.46\cos\left(\frac{2\pi n}{N-1}\right) \qquad (1)$$

was used to extract frequencies, where $N$ is the number of sampling points. We used $N = 128$, which corresponds to 64

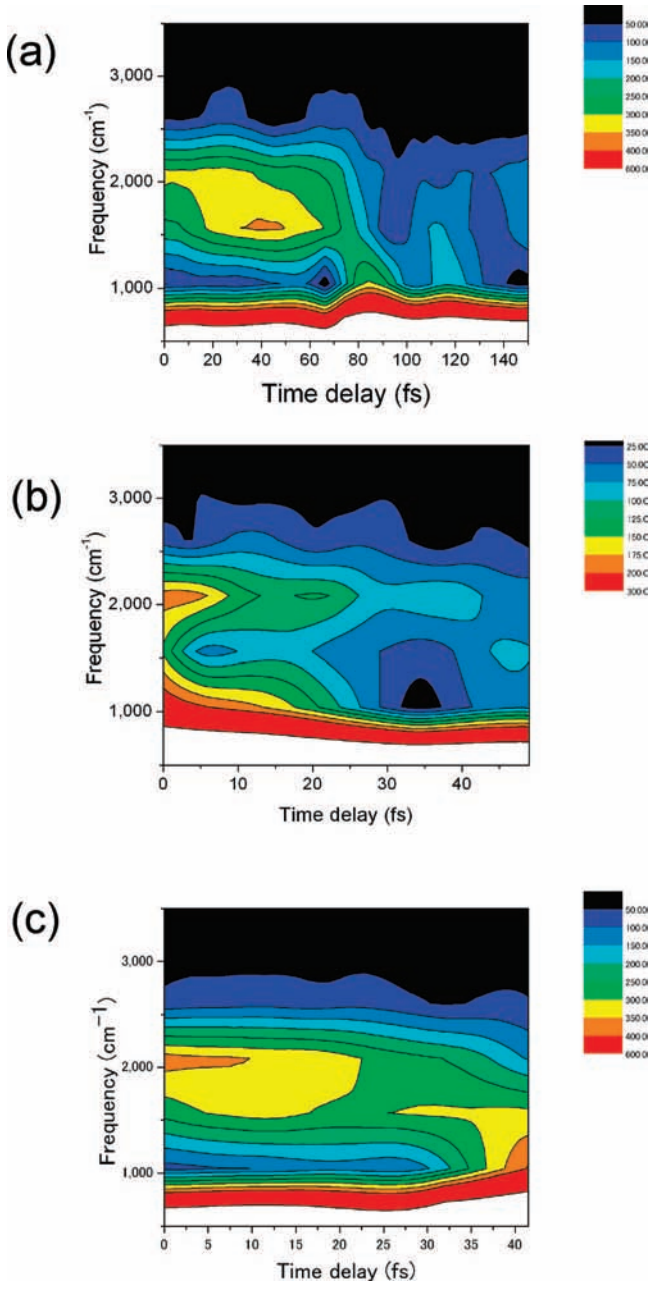


**Figure 7.** Fourier transformation analysis of the typical trajectories used in Figure 4 producing (a) the all-trans form, (b) the 9-cis form, and (c) the 11-cis products in the 12$\pi$ system. The Hamming window function ($w(x) = 0.54 - 0.46\cos(2\pi x)$) for 128 points was used to extract frequencies. The color shows the relative intensity.

fs, to perform fast Fourier transformation in our applications. Figure 7 shows the contour maps from this analysis for the three trajectories shown in Figure 6. The height of the contour map represents the strength of the corresponding vibrational frequency. The time delay $t$ on the $x$-axis means that the time window used spans $t \sim t + 64$ fs.

In Figure 7a, at $t = 0$ there are two peaks, one at $\sim$2000 cm$^{-1}$ and the other at $\sim$0 cm$^{-1}$, which corresponds to low-frequency background. The first peak around 2000 cm$^{-1}$ moves to around 1600 cm$^{-1}$ at $t \approx 20$ fs and fuses into the baseline peak at $\sim$85 fs. In Figure 7b, the frequency of the peak around 2000 cm$^{-1}$ is sustained until 40 fs and then is reduced to about 1600 cm$^{-1}$ or less at 45 fs or later. In Figure 7c, the peak around 2000 cm$^{-1}$ also moves to about 1600 cm$^{-1}$ and fuses into the background. These frequencies, 1600 and 2000 cm$^{-1}$, are close to those of CC conjugate bond stretching[35] and suggest that the molecule in the intermediate state seeks the final stabilized state with the CC conjugate bonds vibrating.

**TABLE 3: The Average Values of Bond Lengths, Absolute Dihedral Angles of the Twisting Bond, Energy Differences between Ground and First Excited States, and the Ground State Energy from the Minimum in Each Cluster in the Simple Cluster Analysis for Metastable Intermediate State and Final Stabilized State in the 12$\pi$ System[a]**

| state | product | $R$ (Å) | $\lvert\phi\rvert$ (deg) | $E_0 - E_1$ (kcal/mol) | $E_0 - E_{min}$ (kcal/mol) |
|---|---|---|---|---|---|
| intermediate (metastable) | trans | 1.459 | 109.9 | −30.2 | 69.5 |
| | 9-cis | 1.476 | 103.9 | −27.9 | 73.8 |
| | 11-cis | 1.464 | 70.5 | −30.0 | 72.5 |
| final (stabilized) | trans | 1.399 | 159.5 | −72.1 | 52.9 |
| | 9-cis | 1.403 | 161.0 | −69.7 | 51.9 |
| | 11-cis | 1.409 | 25.3 | −73.4 | 57.7 |

[a] Each trajectory can be divided into two segments at the energy separation ($E_0 - E_1$) of −50 kcal/mol. $E_0 - E_1 > -50$ kcal/mol ($E_0 - E_1 < -50$ kcal/mol) corresponds to the metastale intermediate (final stabilized) state. $E_{min}$ in the last column is the potential energy of the trans form.

We carried out a simple "cluster analysis" for all trajectory points on the ground state to investigate the metastable intermediate state more closely. All the points of each trajectory in the ground state can be divided into two groups at the energy separation $\Delta E \approx -50$ kcal/mol (see Figure 6). The points with $\Delta E > -50$ ($\Delta E < -50$) kcal/mol correspond to the metastable intermediate (final stabilized) state. In fact, a precise cluster analysis with normalized variables for all the trajectory points of the three trajectories used in Figure 6 leads to almost the same classification. In Table 3, we show the averaged values of the length $R$, the absolute twisting angle $|\phi|$ of the twisting bond, the energy difference between the excited and ground state, and the energy measured from the lowest trans form energy. The averaging was carried out for each cluster of each trajectory and then with respect to the three types of trajectories leading to different products. The averaged $R$ in the intermediate state is 1.46−1.48 Å, which is about 0.06 Å longer than the value 1.40−1.41 Å, which is the bond length of the final stabilized state. Since the typical bond lengths for CC single and double bonds are 1.54 and 1.34 Å,[35] the bond of the intermediate state is single-bond-like and that in the stabilized state is double-bond-like. The averaged $E_0 - E_1$ of the intermediate state is about 40 kcal/mol larger than that of the final stabilized state. The averaged $|\phi|$ are, naturally, significantly different for the intermediate state and the final stabilized state. The average dihedral angle of 110° in the intermediate state becomes wider to 160° in the final all-trans form state, and that of 71° to 25° in the case of the 11-cis form generation. The geometrical parameters in the intermediate state are similar for the 9-cis form generation and all-trans form generation. Thus in the intermediate state the twisting bond has significantly single bond nature and the bond twisting occurs only partially.

One may speculate that the intermediate state corresponds to a certain local minimum separated from the final state by a potential barrier. We have tried to find out whether that is the case or not, starting from tens of trajectory points located in the intermediate state. However, we did not find any local potential minimum for the 11-cis to all-trans isomerization. Thus, it is suggested that the intermediate state is supported by a dynamical barrier due to the multidimensionality.[38] A dynamical barrier is quite common in multidimensional systems, and is observed in the two-dimensional Henon−Heiles potential, for example.[39]

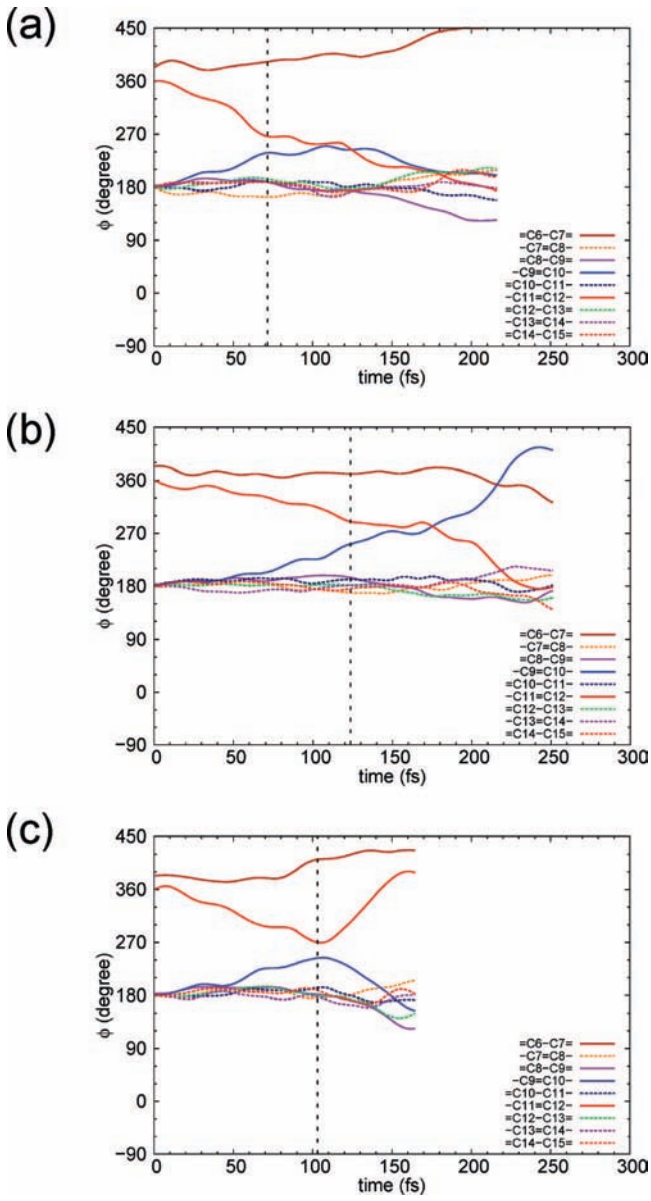


**Figure 8.** The time evolution of dihedral angles of the backbone in retinal. Each trajectory is taken from trajectories that rotate the same direction as retinal in rhodopsin does and that generates (a) the all-trans form, (b) the 9-cis form, and (c) 11-cis form products in the 12$\pi$ system. The vertical dashed line shows the time when the transition occurs. The trajectory is located on the excite state before the transition time and on the ground state after the transition time.

**B. Motion of the Retinal Backbone.** There are several models that have been proposed for the motion of the retinal backbone in the photoisomerization, as described in the Introdution.[7,15−20]

We analyzed the time evolution of dihedral angles related to the backbone CC and CN bonds. In rhodopsin, the initial geometry of photoisomerization is confined by surrounding atoms as the observed crystal structure indicates and would be inclined to rotate the −C11=C12− bond in the counterclockwise direction. Thus, we mainly analyze those trajectories that cause this rotation in the initial stage of time evolution. Figure 8 shows examples of the trajectories to generate the (a) all-trans, (b) 9-cis, and (c) 11-cis forms. Eleven out of all the trajectories calculated give the all-trans form. In 4 out of the 11 trajectories, the −C11=C12− bond rotates in the counterclockwise direction (dihedral angle decreases), which corresponds to the rotation in the rhodopsin protein. The trajectory shown in Figure 8a is one of these four. For all of these four trajectories, the −C9=C10− bond rotates clockwise (dihedral angle increases) up to ∼150 fs, whereas the −C11=C12− bond rotates anticlockwise. Frutos et al. calculated a QM/MM trajectory in rhodopsin, and found a similar correlated change of the two dihedral angles.[7] Weingart et al. also found the crankshaft motion in the five-double-bond model in vacuo without the $\beta$-ionone ring.[8] The present result is consistent with the crankshaft motion. Since the negatively correlated rotation of the −C9=C10− and the −C11=C12− bonds is also found in the present calculations in vacuo, the clockwise rotation of the −C9=C10− bond is considered to be intrinsic in retinal isomerization of the 11-cis form to the all-trans form, which is in agreement with the Weingart's result.

The =C6−C7= bond, which correlates to the motion of the $\beta$-ionone ring, also rotates in the clockwise direction to a small extent compared to the −C9=C10− dihedral angle. However, the =C6−C7= dihedral angle keeps increasing after the transition. This motion would be mainly related to conversion of photon energy to atomic movement in protein. On the ground state, the −C9=C10− dihedral angle goes back to 180°, which is in retard of the motion of the −C11=C12− dihedral angle to the trans form. The =C8−C9= dihedral angle gets smaller in a synchronous way with the recovery of the −C9=C10− dihedral angle to 180°. Thus, this correlated motion of the =C8−C9= angle to the −C9=C10 is a hula-twist type, in which the adjoined double bond and the single bond rotate cooperatively. These motions are common to the four trajectories.

Seven trajectories are found to rotate to the direction opposite to retinal in rhodopsin. In these trajectories, the −C11=C12− bond rotates clockwise and the −C9=C10− bond rotates counterclockwise. On the ground state after transition, the =C8−C9= dihedral angle increases in a synchronous way with the reversion of the adjoined −C9=C10− bond angle to 180°. Thus the hula-twist is again observed here.

In the generation of the 9-cis form the situation is simpler. The −C9=C10− and −C11=C12− bonds rotate in the opposite directions. The other bonds do not move significantly, as shown in Figure 8b. In the reverted 11-cis case (Figure 8c) the rotations of −C11=C12− and −C9=C10− after the transition are just reversal to the 9-cis case.

Overall, the −C9=C10− bond rotates clockwise when the −C11=C12− bond rotates counterclockwise in any routes to the products. Note that the −C9=C10− rotation occurs even when the system goes back to the reactant, the 11-cis form. Since the rotation of the −C9=C10− bond activates the motion directed to the 9-cis form, the channel to the 9-cis form is open in addition to that to the all-trans form. In this sense, the two CI, one between the 11-cis and all-trans forms and the other between the 11-cis and 9-cis forms, are almost equally accessed in vacuo to make a transition to the ground state. In the rhodopsin protein, on the other hand, the 9-cis form is not generated. This indicates that in rhodopsin the route to the 9-cis form is blocked by the surrounding protein and only the route to the all-trans form (and reverted 11-cis form) is left open.

Weingart did not report the 9-cis form generation in his five-double-bond models in vacuo and that the coupled rotation of −C11=C12− and −C9=C10− leading to the 9-cis form is aborted as soon as the molecule returns to the ground state.[8] In the present 12 $\pi$ model, a quarter of trajectory generates the 9-cis form. The difference may be due to the initial condition of dynamics. He used the DFTB/CHarMM optmimized geometry in the binding pocket of rhodopsin, where the −C11=C12−

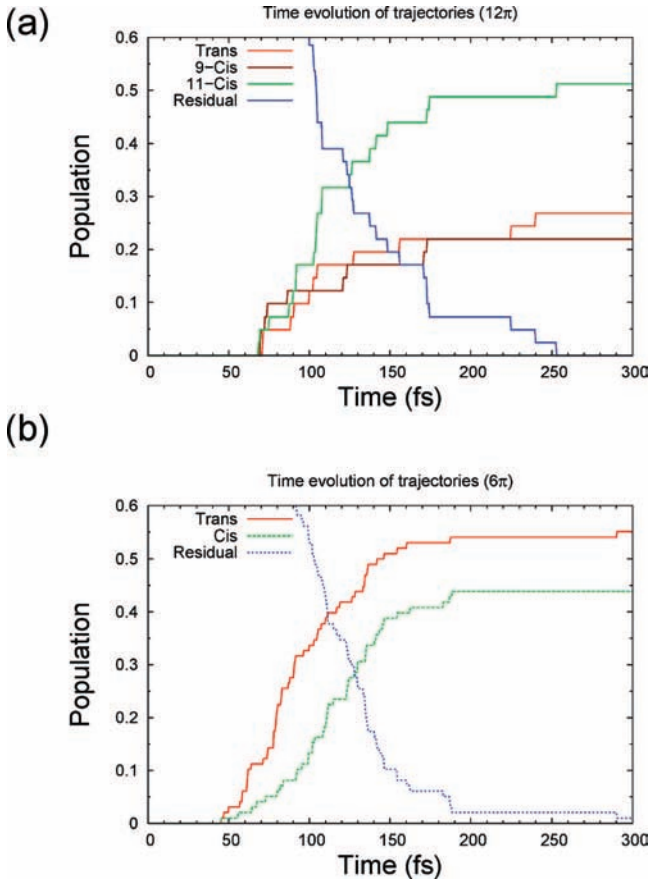


**Figure 9.** Population change estimated from the number of trajectories for $12\pi$ and $6\pi$ systems. Trans- and cis form generations are counted after the transition occurs. The "residual" means the excited cis-state.

dihedral angle of −17.5° and the other dihedral angles twisted the geometry from the plane form significantly. This difference may be seen as an effect of the surrounding protein.

Strambi et al. carried out a QM/MM calculation for isorhodopsin that is a rhodopsin analogue with 9-cis retinal.[21] They postulated that rhodopsin and isorhodopsin relax along a common excited state PES valley starting from opposite ends. The present study suggests a similar common feature for the two proteins. It is shown that the pathway from the 11-cis form to the 9-cis one is open in vacuo, other than to the all-trans one. Figure 2 suggests, furthermore, that the opposite pathway from the 9-cis to the 11-cis form is also open in vacuo. Thus, the 11-cis form generation from isorhodopsin would be hindered by the surrounding protein as hindrance of the 9-cis form in rhodopsin.

**C. Population Change.** Figure 9 shows the population change for both $12\pi$ and $6\pi$ systems. The lifetime of the excited cis form is roughly estimated to be 120−130 fs for both systems. The branching ratio of all-trans, 9-cis, and 11-cis forms at the final stage in the $12\pi$ system is ∼1:1:2. Since the 9-cis form is counted as "trans" with respect to the 11 position, the ratio of the "11-trans" form to the "11-cis" form is ∼5:5 in the $12\pi$ system. The experimental quantum yield of isomerization is 0.67 in protein and 0.15 in solutions.[40,41] Since we can assume safely from the discussion in the previous subsection that the protein environment in rhodopsin suppresses the 9-cis form and leads to the all-trans product, the present result in vacuo is closer to the value in protein. On the other hand, in the $6\pi$ system, the ratio of trans to cis is ∼5.5:4.5, where all the possible forms are only the trans and the (2-)cis forms.

The 11-cis form is produced slightly more than the 11-trans form in the $12\pi$ system, whereas the trans form is produced more in the $6\pi$ model. We have estimated the standard deviation for trans form populations to confirm this tendency. When an equivalent weight is assigned to each trajectory, the (average) population and the standard deviation of population are given by

$$\frac{N_R}{N}$$

and

$$\frac{N_R}{N}\sqrt{\frac{N-N_R}{(N-1)N_R}} = \sqrt{\frac{N_R(N-N_R)}{N^2(N-1)}}$$

where $N$ and $N_R$ are the numbers of total and reactive (trans form) trajectories.[42] The population and its standard deviation for the 11-trans (all-trans or the 9-cis) form are 0.49 (0.56) and 0.08 (0.05) in the $12\pi$ ($6\pi$) system. This is consistent with the above results and the difference between the $12\pi$ and $6\pi$ systems is not significant.

Weingart et al. investigated dynamics of the cis−trans photoisomerization of the present $6\pi$ model with a different nonadiabatic hop scheme and found that 81% of hopped trajectories leaded to the trans form.[43] In their treatment, the hop is determined by the population of the excited and ground states obtained from the projection of the time-dependent electronic Schrödinger equation evolved with classical nuclear propagation. Barbatti et al. also obtained 65% of the trans form.[44] Weingart found that the yield of the trans form is 72% with a five-double-bond model without the $\beta$-ionene ring, which is closer to the present $12\pi$ model. He adopted a method to locate decay points based on the analysis of the configuration interaction vectors.[8,45] The difference of the present result and theirs would be due to the difference in the hopping schemes[8,46,47] and the initial geometry, which was optimized at the level of B3LYP/6-31G in vacuo in the present calculation. The optimized geometry in vacuo would not be suitable for quantitative reproduction of the yield and the B3LYP scheme tends to underestimate the bond-alternation although it is qualitatively correct. One may attribute the difference to the lack of polarization functions of basis sets or the Boltzmann distribution for initial velocities in our calculations, but neither of them would make a major contribution to the difference of branching ratio. We calculated 50 trajectories with the 6-31G(d) set and found a similar population with the present calculation with the 6-31G set in the $6\pi$ system. Their initial conditions were essentially multiple Gaussian distributions at 0 K with zero-point energy whereas we used classical 300 K distribution at the equilibrium geometry, which is also a Gaussian distribution. We estimated Gaussian exponents for the momentum distributions in the $6\pi$ system and the average value is found to be 0.027 and 0.049 for the former and the latter present case, respectively. Thus, our initial distribution is not much different from their initial distributions although the present one is broader. In conclusion, the hopping treatment and the initial geometry employed would be responsible for the difference in branching ratio.

**D. Geometries at the Transition Points.** We investigated the absolute value of the twist angle $|\phi|$ and the angle velocity $d|\phi|/dt$ at the hopping geometries. The transition to the ground

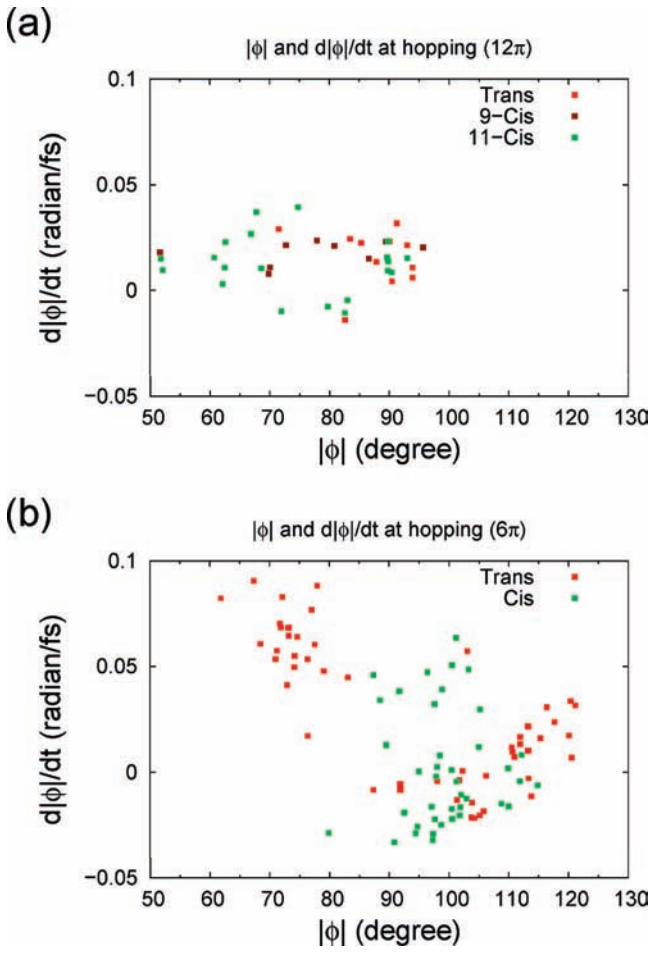


**Figure 10.** Correlation between the absolute value of dihedral angle and its velocity at the transition to the ground state (a) for the $12\pi$ system and (b) for the $6\pi$ system. The green squares are for cis form formation and the red squares are for trans form formation.

state and branching to the final products are determined by the CI between the ground and first excited state. As shown in Figure 3, the CIs correspond to the structure of the dihedral angle of about 90° of the twisting bond in both $6\pi$ and $12\pi$ systems. This suggests that transition occurs when $|\phi| \approx 90°$ and that the trans (cis) product is generated when the transition occurs at $|\phi| \gtrsim 90°$ ($|\phi| \lesssim 90°$).

In the $12\pi$ system, when $|\phi| > 90°$ the all-trans form is mainly generated as expected, although one trajectory $|\phi| > |\phi_{CI}| = 92.5°$ leads to the 9-cis product. As for turning back to the cis form, seven out of nine transitions at $|\phi| < 70°$ lead to the cis form as seen in Figure 10a. Thus, the larger (smaller) values of $|\phi|$ give the trans (cis) form in the $12\pi$ system and this is consistent with the intuitive expectation.

One may also expect that the trans form is mainly generated at positive $d|\phi|/dt$ at the transition, whereas the cis form is generated at negative $d|\phi|/dt$. In the $12\pi$ system, the trajectories with $d|\phi|/dt < 0$ tends to go back to the 11-cis form, which is also consistent with the intuitive expectation. The trajectories with positive $d|\phi|/dt$, however, generate all the three forms; those with smaller $|\phi|$ generate the cis form and those with larger $|\phi|$ generate the all-trans form. It is found that when the cis form generating trajectories with positive $d|\phi|/dt$ are examined in Figure 5a, many of them are repelled in the region of $|\phi| = 70-95°$. In conclusion, the angle of the twisted bond at the hopping geometries mainly controls the final products in the $12\pi$ system.

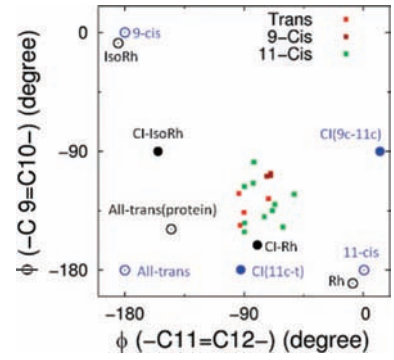


**Figure 11.** Diagram of the twist angles of —C11═C12— and —C9═C10 at the transition points. The minima (open blue circle) and conical intersections (filled blue circle) obtained in the present calculations in vacuo are plotted. The corresponding points in protein obtained by Strambi are also plotted in open and filled black circles. Rh = rhodopsin, IsoRh = isorhodopsin, CI-Rho = CI for conversion of rhodopsin of the 11-cis form to all-trans, and CI-isoRho = CI for conversion of isorhodopsin of the 9-cis form to all-trans.

On the other hand, in the $6\pi$ system, the points are more scattered to both sides of the twist angle ($|\phi_{CI}| = 91.9°$) of the CI structure as seen in Figure 3b and the trans form is generated mainly at $|\phi| > 110°$, whereas the trajectories with $|\phi| < 80°$ interestingly give the trans form. It is also found that the trans form products are mainly generated when angle velocities are positive and the cis form products are mainly generated when the angle velocities are negative, which is in agreement with the intuitive expectation.

We also investigated the length of twisting bond $R$ at the transition and found that $R$ is distributed in a narrower range in the $12\pi$ system than in the $6\pi$ system. Namely, the transitions occur nearer the CI in the former system, whereas the transition points are more scattered in a wider range in the latter system.

Strambi et al. showed a topology map of rhodopsin, isorhodopsin, and conical intersections that were obtained from their QM/MM calculations.[21] Figure 11 is a similar diagram for the transition points. The diagram also includes the points for rhodopsin and isorhodopsin and the conical intersections in protein obtained by Strambi et al. The minima and CI are located almost at some of the grid points every 90° in vacuo whereas the corresponding points in protein are located on a curve or nearer the curve, as pointed out by Srambi et al. This may indicate that protein force fields result in facilitating desirable reactions. The ranges of the two angles at the transition are $-94° < \phi(-C11{=}C12-) < -52°$ and $-151° < \phi(-C9{=}C10-) < -107°$. Thus, the amount of (clockwise) rotation of $\phi$(—C9═C10—) (29 to 73°) is smaller than that of (counterclockwise) $\phi$(—C11═C12—) rotation (52 to 94°). The transition point generating the all-trans form is distributed near the CI between the 11-cis and all-trans form (CI(11c-t)). The CI in protein is closer than that in vacuo to the distribution of transition points. This suggests that the yield of the trans form would be larger in protein than in vacuo. The point leading to the 9-cis form is slightly closer to the CI between the 9-cis and 11-cis forms (CI(9c−11c)) although the trend is less clear than the case for the all-trans generation.

## Conclusions

Ab initio nonadiabatic classical dynamics calculations have been carried out for two models of protonated Schiff base retinal, the $6\pi$ model, PSB3 and the $12\pi$ model, PSB of retinal in which two methyl groups are removed from the Schiff base. The

**SCHEME 1: Overall Mechanism of the Isomerization in the Case of the 12$\pi$ System**

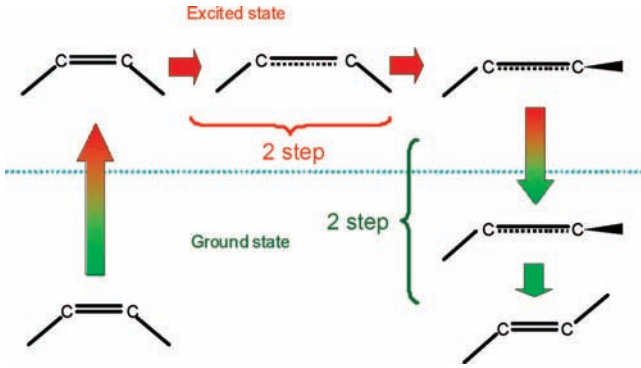


probabilities of nonadiabatic transition between the excited and ground states were estimated by the Zhu−Nakamuara formulas. The 9-cis form product in addition to the all-trans one is generated in the present gas-phase calculation for the 12$\pi$ model. It is suggested, therefore, that, in rhodopsin, the path to the 9-cis product is suppressed by the surrounding protein.

We have found that energy relaxation on the ground state occurs in two steps in the 12$\pi$ model. This relaxation pattern can be seen in the all-trans and 9-cis products as well as in the reverted 11-cis form. Fourier transformation analysis reveals that the effective vibrational frequencies of the intermediate state are 1600−2000 $cm^{-1}$, which is assigned to the conjugate CC bond frequencies in the ground electronic state. It is suggested that the intermediate state and the final stabilized states are separated by a dynamical barrier due to the multidimensionality and that the molecule in the intermediate state waits for a while to cross this barrier. This two-step relaxation mechanism on the ground electronic state is schematically depicted in Scheme 1 and summarized as follows: (1) The twisting bond vibrates about 130 fs keeping the single bond character. (2) The energy relaxes further and the twisting bond shrinks to the double bond and the trans form or cis form is finally generated.

The decrease (increase) of the −C11═C12− bond dihedral angle with time is accompanied with increase (decrease) of the −C9═C10− one in generation of the all-trans form, which shows the latter change is intrinsic in retinal isomerization, not due to restraint from surrounding protein. In any reaction paths, the −C11═C12− angle change is accompanied by the −C9═C10− angle change in the opposite direction, which leads to all-trans, 9-cis, and (reverted) 11-cis forms.

The branching into the final products is mainly determined by the twist angle at the hopping geometries in the 12$\pi$ system, although the correlation between the angle at the hopping and the product is not very strong.

The blocking of the 9-cis formation in rhodopsin may suggest that there is similar blocking of the 11-cis formation of isorhodopsin. If we assume a distribution of transition points in 9-cis retinal is similar to the 11-cis case, the transition points would distribute symmetrically with the 11-cis transition points with respect to the 45° line (where $\phi$(−C9═C10−) = $\phi$(−C11═C12−)) in Figure 11. These transition points for the 9-cis form are farther away from the conical intersection between the 9-cis and 11-cis forms (CI(9c−11c)) than those for the 11-cis form. Thus, the conversion of the 9-cis form to the 11-cis form may be intrinsically forbidden in retinal, not due to the isorhodopsin environment, which is different from the rhodopsin case, although dynamics calculations are needed to confirm this conjecture.

**Acknowledgment.** This study was supported by a Grant-in-Aid for Specially Promoted Research on "Studies of Nonadiabatic Chemical Dynamics based on the Zhu-Nakamura Theory" (No. 15002011) and Scientific Research (B) (No. 19350013) from MEXT, Japan. T.I. and S.N. also acknowledge support by a Grant-in-Aid for Scientific Research (C) (Nos. 16550025 and 20608003). A portion of the computations were carried out at the Research Center for Computational Science, Okazaki, Japan.

## References and Notes

(1) Okada, T.; Ernst, O. P.; Palczewski, K.; Hofmann, K. P. *Trends Biochem. Sci.* **2001**, *26*, 318–324.
(2) Sakmar, T. P.; Menon, S. T.; Marin, E. P.; Awad, E. S. *Annu. Rev. Biophys. Biomol. Struct.* **2002**, *31*, 443–484.
(3) Burns, M. E.; Baylor, D. A. *Annu. Rev. Neurosci.* **2001**, *24*, 779–805.
(4) Hubbell, W. L.; Altenbach, C.; Hubbell, C. M.; Khorana, H. G. *Adv. Protein Chem.* **2003**, *63*, 243–290.
(5) Wanko, M.; Hoffmann, M.; Frauenheim, T. J.; Elstner, M. *J. Comput. Aided Mol. Des.* **2006**, *20*, 511–518.
(6) Vreven, T.; Morokuma, K. *J. Chem. Phys.* **2000**, *113*, 2969–2975.
(7) Frutos, L. M.; Andruniów, T.; Santoro, F.; Ferrœe, N.; Olivucci, M. *Proc. Natl. Acad. Sci. U.S.A.* **2007**, *104*, 7764–7769.
(8) Weingart, O. *J. Am. Chem. Soc.* **2007**, *129*, 10618–10619.
(9) Schapiro, I.; Weingart, O.; Buss, V. *J. Am. Chem. Soc.* **2009**, *131*, 16–17.
(10) Nakamura H. *Nonadiabatic Transitions, Concepts, Basic Theories and Applications*; World Scientific: Singapore, 2002.
(11) Zhu, C.; Nakamura, H. *J. Chem. Phys.* **1994**, *101*, 4855–4866. Zhu, C.; Nakamura, H. *J. Chem. Phys.* **1994**, *101*, 10630–10647. Zhu, C.; Nakamura, H. *J. Chem. Phys.* **1995**, *102*, 7448–7461.
(12) Nakamura, H. *J. Theor. Comput. Chem.* **2005**, *4*, 127–137.
(13) Nakamura, H. *Adv. Chem. Phys.* **2008**, *138*, 95–212.
(14) Landau, L. *Phys. Z. Soviet.* **1932**, *2*, 46–51. Zener, C. *Proc. R. Soc. London A* **1932**, *137*, 696–702. Stückelberg, E. C. G. *Helv. Phys. Acta* **1932**, *5*, 369.
(15) Kakitani, T.; Kakitani H., *J. Phys. Soc. Jpn.* **1975**, *38*, 1455–1463.
(16) Warshel, A. *Nature* **1976**, *260*, 679–683.
(17) Liu, R. S. H.; Asato, A. E. *Proc. Natl. Acad. Sic. U.S.A.* **1985**, *82*, 259–263.
(18) Liu, R. S. H.; Browne, D. T. *Acc. Chem. Res.* **1986**, *19*, 42–48.
(19) Liu, R. S. H.; Hammond, G. S. *Proc. Natl. Acad. Sic. U.S.A.* **2000**, *97*, 11153–11158.
(20) Yamada, Y.; Yamato, T.; Kakitani, T.; Yamamoto, S. J. *Photoscience* **2002**, *9*, 51–54.
(21) Strambi, A.; Coto, P. B.; Frutos, L. M.; Ferre, N.; Olivucci, M. *J. Am. Chem. Soc.* **2008**, *130*, 3382–3388.
(22) *MOLPRO*, version 2006.1, a package of ab initio programs designed by:Werner, H.-J.; Knowles, P. J.; Lindh, R.; Manby, F. R.; Schütz, M.; Celani, P.; Korona, T.; Rauhut, G.; Amos, R. D.; Bernhardsson, A.; Berning, A.; Cooper, D. L.; Deegan, M. J. O.; Dobbyn, A. J.; Eckert, F.; Hampel, C.; Hetzer, G.; Lloyd, A. W.; McNicholas, S. J.; Meyer, W.; Mura, M. E.; Nicklass, A.; Palmieri, P.; Pitzer, R.; Schumann, U.; Stoll, H.; Stone, A. J.; Tarroni, R.; Thorsteinsson, T.; 2006; http://www.molpro.net.
(23) *MOLPRO*, version 2002.6, a package of ab initio programs designed by: Werner, H.-J.; Knowles, P. J.; Amos, R. D.; Bernhardsson, A.; Berning, A.; Celani, P.; Cooper, D. L.; Deegan, M. J. O.; Dobbyn, A. J.; Eckert, F.; Hampel, C.; Hetzer, G.; Knowles, P. J.; Korona, T.; Lindh, R.; Lloyd, A. W.; McNicholas, S. J.; Manby, F. R. ; Meyer, W.; Mura, M. E.; Nicklass, A.; Palmieri, P.; Pitzer, R.; Rauhut, G.; Schütz, M.; Schumann, U.; Stoll, H.; Stone, A. J.;Tarroni, R.; Thorsteinsson, T.; Werner, H.-J., 2003; http://www.molpro.net.
(24) Frisch, M. J.; Trucks, G. W.; Schlegel, H. B.; Scuseria, G. E.; Robb, M. A.; Cheeseman, J. R.; Montgomery, J. A., Jr.; Vreven, T.; Kudin, K. N.; Burant, J. C.; Millam, J. M.; Iyengar, S. S.; Tomasi, J.; Barone, V.; Mennucci, B.; Cossi, M.; Scalmani, G.; Rega, N.; Petersson, G. A.; Nakatsuji, H.; Hada, M.; Ehara, M.; Toyota, K.; Fukuda, R.; Hasegawa, J.; Ishida, M.; Nakajima, T.; Honda, Y.; Kitao, O.; Nakai, H.; Klene, M.; Li, X.; Knox, J. E.; Hratchian, H. P.; Cross, J. B.; Bakken, V.; Adamo, C.; Jaramillo, J.; Gomperts, R.; Stratmann, R. E.; Yazyev, O.; Austin, A. J.; Cammi, R.; Pomelli, C.; Ochterski, J. W.; Ayala, P. Y.; Morokuma, K.; Voth, G. A.; Salvador, P.; Dannenberg, J. J.; Zakrzewski, V. G.; Dapprich, S.; Daniels, A. D.; Strain, M. C.; Farkas, O.; Malick, D. K.; Rabuck, A. D.; Raghavachari, K.; Foresman, J. B.; Ortiz, J. V.; Cui, Q.; Baboul, A. G.; Clifford, S.; Cioslowski, J.; Stefanov, B. B.; Liu, G.; Liashenko, A.; Piskorz, P.; Komaromi, I.; Martin, R. L.; Fox, D. J.; Keith, T.; Al-Laham, M. A.; Peng, C. Y.; Nanayakkara, A.; Challacombe, M.; Gill, P. M. W.; Johnson, B.; Chen, W.; Wong, M. W.; Gonzalez, C.; Pople, J. A. *Gaussian 03*, Revision C.02; Gaussian, Inc., Wallingford, CT, 2004.

(25) Swope, W. C.; Andersen, H. C.; Berens, P. H.; Wilson, K. R. *J. Chem. Phys.* **1982**, *76*, 637–649.
(26) Zhu, C.; Nobusada, K.; Nakamura, H. *J. Chem. Phys.* **2001**, *115*, 3031–3044.
(27) Li, B.; Han, K.-L. *J. Chem. Phys.* **2008**, *128*, 114116/1–7.
(28) Zhu, C.; Kamisaka, H.; Nakamura, H. *J. Chem. Phys.* **2001**, *115*, 11036–11039.
(29) Zhu, C.; Kamisaka, H.; Nakamura, H. *J. Chem. Phys.* **2002**, *116*, 3234–3247.
(30) Oloyede, P.; Mil'nikov, G.; Nakamura, H. *J. Chem. Phys.* **2006**, *124*, 144110/1–11.
(31) Photodissociation of $BrCH_2COCl$: Zhang, F.; Ding, W-J.; Fang, W.-H. *J. Chem. Phys.* **2006**, *125*, 184305/1–7.
(32) Hubbard, R.; Kropf, A. *Proc. Natl. Acad. Sci. U.S.A.* **1958**, *44*, 130–139.
(33) Kochendoerfer, G. G.; Mathies, R. A. *J. Phys. Chem.* **1996**, *100*, 14526–14532.
(34) Vreven, T.; Bernardi, F.; Graveilli, M.; Olivucci, M.; Robb, A. A.; Schlegel, H. B. *J. Am. Chem. Soc.* **1997**, *119*, 12687–12688.
(35) Atkins, P. W. *Physical Chemistry*, 6th ed.; Oxford University Press: Oxford, UK, 1998.
(36) González-Luque, R; Garavelli, M; Bernardi, F.; Merchán, M.; Robb, M. A.; Olivucci, M. *Proc. Natl. Acad. Sci. U.S.A.* **2000**, *97*, 9379–9384.
(37) BlackmanR. B.; TukeyJ. W. *The Measurement of Power Spectra*; Dover: New York , 1958; Appendix B.5, pp 95−100. Harris, F. J. *Proc. IEEE* **1978**, *66*, 51.
(38) Miller W. H. Classical-Limit Quantum Mechanics and the Theory of Molecular Collisions. In *Advances in Chemical Physics*; Prigogine, I., Rice, S. A., Eds.; Wiley: New York, 1974; Vol *XXV* pp. 69177.
(39) Hutchinson, J. S.; Wyatt, R. E. *Phys. Rev. A* **1981**, *23*, 1567–1584.
(40) Hurley, J. B.; Ebrey, T. G.; Ilonig, B.; Ottolenghi, M. *Nature* **1977**, *270*, 540–542.
(41) Koyama, Y.; Kubo, K.; Komori, M.; Yasuda, H.; Mukai, Y. *Photochem. Photobiol.* **1991**, *54*, 433–443.
(42) Mayne H. R. The Classical Trajectory Approach to Reaction Dynamics In *Dynamics of Molecules and Chemical Reactions*; Wyatt R. E., Zhang J. Z. H., Eds.; Marcel Dekker, Inc.: New York, 1996; Chapter 15, p 589.
(43) Weingart, O.; Migani, A.; Olivucci, M.; Robb, M. A.; Buss, V.; Hunt, P. *J. Phys. Chem. A* **2004**, *108*, 4685–4693.
(44) Barbatti, M.; Ruckenbauer, M.; Szymczak, J. J.; Aquino Adelia, J. A.; Lischka, H. *Phys. Chem. Chem. Phys.* **2008**, *10*, 482–494.
(45) Groenhof, G.; Bouxin-Cademartory, M.; Hess, B.; De Visser, S. P.; Berendsen, H. J. C.; Olivucci, M.; Mark, A. E.; Robb, M. A. *J. Am. Chem. Soc.* **2004**, *126*, 4228–4233.
(46) Klein, S.; Bearpark, M. J.; Smith, B. R.; Robb, M. A.; Olivucci, M.; Bernardi, F. *Chem. Phys. Lett.* **1981**, *292*, 259–266.
(47) Barbatti, M.; Granucci, G.; Persico, M.; Ruckenbauer, M.; Vazdar, M.; Eckert-Maksić, M.; Lischka, H. *J. Photochem. Photobiol. A* **2007**, *190*, 228–240.

JP8110315